Applied Physics Letters

# Invar effects of $(Fe_{71.2}B_{24}Y_{4.8})_{96}Nb_4$ alloy in different structural states

Cite as: Appl. Phys. Lett. **97**, 221907 (2010); https://doi.org/10.1063/1.3524199
Submitted: 10 October 2010 . Accepted: 11 November 2010 . Published Online: 01 December 2010

Qiang Hu, Xie-Rong Zeng, and Ming-Wang Fu

# Invar effects of $(Fe_{71.2}B_{24}Y_{4.8})_{96}Nb_4$ alloy in different structural states

Qiang Hu,[1] Xie-Rong Zeng,[2,3,a)] and Ming-Wang Fu[4]
[1]*School of Materials Science and Engineering, Northwestern Polytechnical University, Xi'an, Shannxi 710072, People's Republic of China*
[2]*College of Materials Science and Engineering, Shenzhen University, Shenzhen 518060, People's Republic of China*
[3]*Shenzhen Key Laboratory of Special Functional Materials, Shenzhen 518060, People's Republic of China*
[4]*Department of Mechanical Engineering, The Hong Kong Polytechnic University, Hong Kong*

(Received 10 October 2010; accepted 11 November 2010; published online 1 December 2010)

This paper reports the observation of the clear Invar effects of $(Fe_{71.2}B_{24}Y_{4.8})_{96}Nb_4$ bulk metallic glass. The Invar effects of $(Fe_{71.2}B_{24}Y_{4.8})_{96}Nb_4$ alloys in different structural states are also investigated *in situ* through cyclic thermal dilation tests at different cyclic temperatures. The results show that these Invar effects are strengthened in the relaxation amorphous state, weakened in the nanocrystalline state, and absent in the complete crystalline state. X-ray diffraction and Mössbauer spectroscopy demonstrate that the structural influences on Invar effects can be explained by the different local atomic arrangements around Fe atoms in different structural states. © *2010 American Institute of Physics*. [doi:10.1063/1.3524199]

Invar effects constitute one of the most fundamental research topics in the area of magnetism,[1,2] and numerous iron-based amorphous ribbons that exhibit such effects have been investigated in recent years.[3–6] A small thermal expansion coefficient in the order of $10^{-6}$ $K^{-1}$ below the Curie temperature, analogous to crystalline $Fe_{65}Ni_{35}$, has been reported for these amorphous ribbons, although their potential as commercial low-expansion alloys is limited by their small dimension (typically 50 $\mu$m) and low Curie temperature (lower than 400 K). Recently, however, a class of Fe–B–Y–Nb soft magnetic bulk metallic glass (BMG) with strong glass-forming ability (critical diameter is 7 mm), high Curie temperature (higher than 450 K), excellent thermal stability (large supercooled liquid region with a temperature interval of about 90 K), and high compressive fracture stress (4 GPa) has been obtained.[7] This paper reports the observation of the clear Invar effects of $(Fe_{71.2}B_{24}Y_{4.8})_{96}Nb_4$ BMG.[8] The Invar effects of $(Fe_{71.2}B_{24}Y_{4.8})_{96}Nb_4$ alloys in different structural states are also investigated.

$(Fe_{71.2}B_{24}Y_{4.8})_{96}Nb_4$ master alloys were prepared by arc melting the pure element mixture in a Ti-gettered high-purity argon atmosphere. Amorphous ribbons (20 $\mu$m $\times$ 1 mm) and rods ($\Phi$2.5 mm $\times$ 50 mm) were prepared via single-roller melt spinning and copper-mold casting, respectively. The BMG rods ($\Phi$2.5 mm $\times$ 25 mm) and master alloy ingot (2.5 $\times$ 2.5 $\times$ 25 mm) were tested in a thermal dilatometer (DIL; Netzsch DIL 402C) in an argon atmosphere. The load applied on the samples was 0.3 N, and the instrument resolution was 1.25 nm. The thermal electric resistance of the BMG rods ($\Phi$2.5 mm $\times$ 20 mm) was tested in a helium atmosphere using the dc four-probe technique (TER; ULVKC-RIKO ZEM-2), and their thermomagnetic curve was tested with a vibrating sample magnetometer (TM; Nanjing University, VSM-HH20). The BMG rods' glass transition and crystallization behaviors were evaluated using differential scanning calorimetry (DSC) (Setaram SETSYS Evolution 1750). The ribbons that sealed in vacuum quartz tubes (4 $\times 10^{-3}$ Pa) and the rods were isochronal-annealed in a muffle furnace and a thermal dilatometer in an argon atmosphere, respectively. The heating rate of all of the thermoanalysis tests and isochronal annealing was 0.0833 K/s, and the cross sections of the rods and the ribbon surfaces were investigated via x-ray diffraction (XRD) (Bruker D8). Finally, the transmission Mössbauer spectra (OXFORD MS-500) of the ribbons were obtained at room temperature with a $^{57}$Co/Pd source. Calibration of the spectrometer is referred to as $\alpha$-Fe at 293 K.

In addition to the small thermal expansion coefficient $\alpha$ in the order of $10^{-6}$ $K^{-1}$ below the Curie temperature, the Invar abnormities of amorphous alloys also display in a minimum electrical resistivity around the Curie temperature. As shown in Fig. 1(a), the Curie temperature, identified as the minima in the first derivative of the $M/M_0$-$T$ curve, is

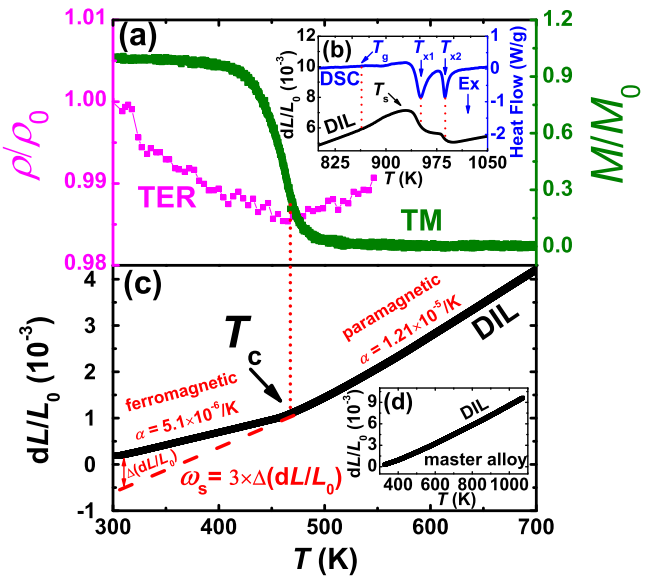


FIG. 1. (Color online) (a) Reduced TER and TM traces of $(Fe_{71.2}B_{24}Y_{4.8})_{96}Nb_4$ amorphous rods; (b) glass transition temperature $T_g$, crystallization peak temperature $T_x$, and softening temperature $T_s$ measured by DSC and DIL and DIL traces of (c) amorphous rods and (d) master alloy.

a)Electronic mail: zengxier@szu.edu.cn.

 

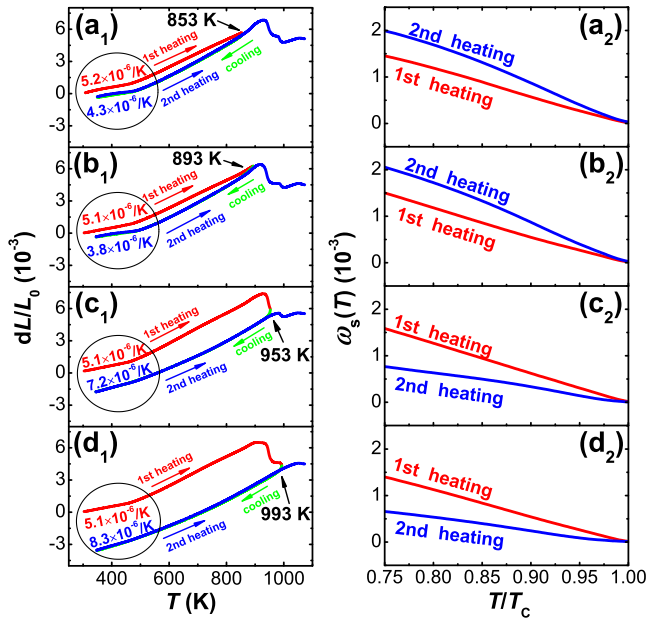


FIG. 2. (Color online) [(a1)–(d1)] Cyclic DIL traces with different cyclic temperatures of amorphous rods (the Invar effects are marked by circles and the average $\alpha$ in the first and second heating are also given); [(a2)–(d2)] corresponding $\omega_s(T)$ vs $(T/T_c)$ curves.

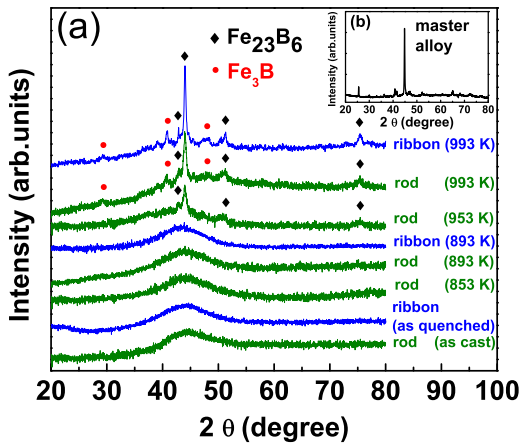


FIG. 3. (Color online) (a) XRD of rods and ribbons after isochronal annealing; (b) master alloy.

470 K. Electrical resistivity has a minimum at 464 K. The relative value of electrical resistivity decreases by 1.5% compared to that at room temperature, which is similar to amorphous Fe–(Ni,Co)–Zr ribbons with clear Invar effects.[5,9] Figure 1(c) shows that an abrupt increase at 465 K occurs in the DIL trace. The average $\alpha$ in the ferromagnetic (below 465 K) and paramagnetic (above 470 K) phases is in the same order as that in other amorphous Invar ribbons[3–6] and nonmagnetic BMGs,[10,11] respectively. A large degree of spontaneous volume magnetostriction $\omega_s$ ($1.5\times10^{-3}$ at room temperature), which is estimated as the treble of the thermal expansion difference between the ferromagnetic phase and the oppositely elongated line of the paramagnetic phase,[12] can be seen clearly in Fig. 1(c). In summary, the unusual thermal behaviors prove the existence of clear Invar effects in $(Fe_{71.2}B_{24}Y_{4.8})_{96}Nb_4$ BMG.[8]

An interesting observation from Fig. 1(d) is that there is no obvious Invar abnormality in the master alloy with coarse grains. It is well known that amorphous alloys do not have a structure with a long-range atomic order as do crystalline materials, but rather a pronounced short-range order at the atomic scale.[13] To further investigate the local atomic arrangement influences on the Invar effects, the rods' thermal expansions in different structural states were measured *in situ* by cyclic DIL tests at different cyclic temperatures. The glass transition point $T_g$ and first and second crystallization peaks, $T_{x1}$ and $T_{x2}$, were observed by DSC at 862, 951, and 984 K, respectively. The softening temperature $T_s$ (the temperature corresponding to the maximum point of the thermal expansion curve) is 918 K.[10,11] As shown in Figs. 2(a1)–2(d1), the cyclic temperatures were 853 K (853 K$<T_g$), 893 K ($T_g<893$ K$<T_s<T_{x1}$), 953 K ($T_s<T_{x1}<953$ K$<T_{x2}$), and 993 K (993 K$>T_{x2}$), respectively. Hence, after the initial heating and cooling processes shown in Figs. 2(a1)–2(d1), the rods were in different structural states prior to the second heating. Because of the free volume annihilation in the first heating shown in Figs. 2(a1)–2(d1) and the viscous flows shown in Figs. 2(c1)–2(d1), there was a degree of vertical distance between the first heating and cooling DIL trace in each test. The viscous flows that can be seen in Figs. 2(c1)–2(d1) are very small (the length shrinkage is about 1‰–3‰) (Refs. 10 and 11) and thus should not affect the shape of the cylinder samples violently; hence, the $\omega_s$ of the second heating can still be estimated from Fig. 1(c). The cooling curve and second heating curve almost overlap in each test also because of the free volume annihilation, although the transition is from the ferromagnetic phase to the paramagnetic phase in heating and vice versa in cooling. Thus, for accurate comparison, only the $\omega_s$ of the first and second heating, as a function of the reduced Curie temperature, are shown in Figs. 2(a2)–2(d2). The $\omega_s(T)$ of the second heating in Figs. 2(a2)–2(b2) and in Figs. 2(c2)–2(d2) are larger and smaller than those of the corresponding first heating, respectively. Hence, the Invar effects are strengthened and weakened after relaxation below and above $T_{x1}$, respectively. This regularity is also confirmed by the average $\alpha$ in the ferromagnetic phase as indicated in Figs. 2(a1)–2(d1). The $\alpha$ decreases in Figs. 2(a1)–2(b1) and increases in Figs. 2(c1)–2(d1).

Figure 3 shows the XRD of additional rods that underwent the same initial heating and cooling procedure as those in Figs. 2(a1)–2(d1). The rods remained amorphous after isochronal annealing to 853 and 893 K, although some nanocrystalline behavior appeared after isochronal annealing to 953 and 993 K. In observing Fig. 3, it is difficult to explain why the Invar effects are strengthened or weakened in different structural states. As it is well known that such effects are closely related to the internal magnetic structure, Mössbauer spectroscopy, one of the most powerful methods for structural investigations of amorphous and nanocrystalline alloys was carried out on the $(Fe_{71.2}B_{24}Y_{4.8})_{96}Nb_4$ ribbons in different structural states.

The Mössbauer spectra in Figs. 4(a1) and 4(b1) consist of very broad and overlapping lines, typical of the amorphous systems confirmed by XRD.[14,15] Isochronal annealing of the ribbons to 993 K leads to the appearance of hyperfine sextets with sharp lines superimposed on the broad lines, as shown in Fig. 4(c1). This is typical of nanocrystalline decomposition of the amorphous matrix, which is also consistent with XRD.[14,15] The hyperfine field distributions in Figs. 4(a2)–4(c2) exhibit bimodal profiles and can be fitted by two

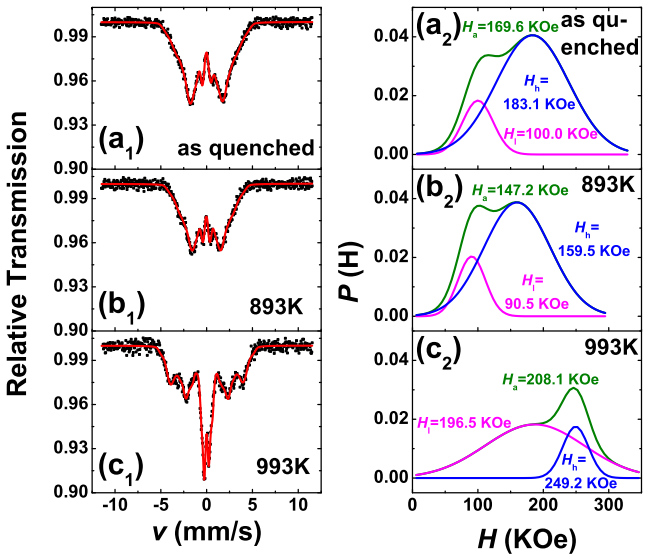


FIG. 4. (Color online) Mössbauer spectra [(a1), (b1), and (c1)] and corresponding hyperfine field distributions [(a2), (b2), and (c2)] of $(Fe_{71.2}B_{24}Y_{4.8})_{96}Nb_4$ ribbons in the as-quenched state and different isochronal annealing states. $H_a$, $H_l$, $H_h$ is the average hyperfine field and low- and high-field components, respectively.

Gaussian distributions, which indicates the presence of two different local magnetic environments for the Fe atoms. The high- and low-field components, respectively, are attributed to the Fe-poor regions, in which the Fe atoms are partially coordinated with the B, Y, and Nb nonmagnetic atoms and the Fe-rich regions, in which the Fe atoms are mainly surrounded by other Fe atoms with a certain distribution of the Fe–Fe nearest neighbors' distances.[16] Because of the dependence of the exchange interaction between two Fe atoms on their separation, the spatial fluctuations of the interatomic distances lead to competing ferromagnetic (for larger distances) and antiferromagnetic (for smaller distances) interactions.[17] After isochronal annealing to 893 K, the sample is still amorphous, although it has a more closely packed structure due to the free volume annihilation. The enhancement of atom packing density results in a decrease in the Fe–Fe nearest neighbors' distance and therefore the weakening of the ferromagnetic coupling between Fe–Fe atoms.[14,15] Hence, compared to the as-quenched sample, there is a decrease in the low-field as indicated in Figs. 4(a2) and 4(b2). It is well known that the low-field component is responsible for the Invar effect,[17] and thus a decrease in the low field enhances this effect. However, $Fe_{23}B_6$ and $Fe_3B$ nanocrystalline behavior is displayed in the amorphous matrix after isochronal annealing to 993 K. The increased ordering of the Fe atoms with nonmagnetic B atoms results in an increase in the high field and a decrease in the low field.[14,15] Consequently, the Invar effects are suppressed. Finally, in the master alloy with coarse grains and no amorphous phase, the long-range order of the Fe atoms with other nonmagnetic atoms leads to the disappearance of the Invar effects.

In summary, this paper represents the observation of clear Invar effects in a BMG. Invar effects are strengthened after relaxation below the crystalline temperature because of the decrease in Fe–Fe nearest neighbors' distance due to free volume annihilation, weakened when nanocrystalline behavior occurs in the amorphous matrix because of the increased ordering of the Fe atoms with other nonmagnetic atoms, and completely disappear in the master alloy with coarse grains and no amorphous phase. The strong glass-forming ability, high Curie temperature, and excellent mechanical properties of $(Fe_{71.2}B_{24}Y_{4.8})_{96}Nb_4$ BMG, combined with its clear Invar effects, shed light on the development of low-expansion BMG.

This research was conducted with financial support from the Science and Technology Foundation of Shenzhen China (Grant No. CXB200903090012A) and the Two Hundred Plans for Talent Station of Shenzhen (Shenfu [2008] Grant No. 182).

[1]R. Kainuma, J. J. Wang, T. Omori, Y. Sutou, and K. Ishida, Appl. Phys. Lett. **80**, 4348 (2002).
[2]M. van Schilfgaarde, I. A. Abrikosov, and B. Johansson, Nature (London) **400**, 46 (1999).
[3]Z. Xianyu, Y. Ishikawa, S. Ishio, and M. Takahashi, J. Phys. F: Met. Phys. **15**, 1787 (1985).
[4]G. Vlasak, P. Duhaj, and P. Svec, J. Magn. Magn. Mater. **140–144**, 443 (1995).
[5]Z. Xianyu, J. Z. Li, Z. C. Lu, J. Kang, C. T. Ye, and Z. Q. Li, Physica B **213–214**, 535 (1995).
[6]P. Kamasa and P. Myśliński, Cent. Eur. J. Phys. **4**, 178 (2006).
[7]D. H. Kim, J. M. Park, and W. T. Kim, J. Mater. Res. **22**, 471 (2007).
[8]M. Hatate, J. S. Garitaonandia, and K. Suzuki, J. Appl. Phys. **103**, 07B909 (2008).
[9]K. Shirakawa, K. Fukamichi, T. Kaneko, and T. Masumoto, J. Phys. F: Met. Phys. **14**, 1491 (1984).
[10]H. S. Chen, J. Appl. Phys. **49**, 3289 (1978).
[11]X. H. Chen, Y. Zhang, G. L. Chen, X. C. Zhang, and L. Liu, J. Appl. Phys. **103**, 113506 (2008).
[12]J. L. Wang, M. R. Ibarra, C. Marquina, B. Garcia-Landa, O. Tegus, Q. F. Xiao, E. Bruck, F. M. Yang, and G. H. Wu, J. Appl. Phys. **91**, 8216 (2002).
[13]N. Jakse and A. Pasturel, Appl. Phys. Lett. **93**, 113104 (2008).
[14]J. Olszewski, J. Zbroszczyk, H. Fukunaga, W. Ciurzynska, J. Swierczek, M. Hasiak, K. Perduta, A. Lukiewska, and A. Mlynczyk, Nukleonika **49**, S79 (2004).
[15]J. Olszewski, Hyperfine Interact. **131**, 83 (2000).
[16]K. Brzozka, A. Slawska-Waniewska, P. Nowicki, and K. Jezuita, Mater. Sci. Eng., A **226–228**, 654 (1997).
[17]V. A. Makarov, A. Y. Belenkii, and O. S. Kozlova, Phys. Status Solidi A **139**, 173 (1993).